

White Spaces Pattern Finding and Inference based on Machine Learning for Multi-frequency Spectrum Footprints

Rodney Martinez Alonso*, David Plets, Luc Martens, Wout Joseph

Ghent University, Technologiepark 126, 9052 Ghent, Belgium

Ernesto Fontes Pupo

University of Cagliari, Piazza D'Armi – 09123 Cagliari, Italy

Glauco Guillen Nieto

LACETEL, 34515 Independencia Ave., 19200 Havana, Cuba

Abstract

Spectrum surveys performed worldwide demonstrate that the spectrum utilization efficiency is less than 0.25. Therefore, the traditional long-term licensed spectrum allocation by regulators is not sustainable. Although dynamic spectrum access networks allow increasing the efficiency of spectrum utilization, coexistence is still a major problem. In this paper, we investigate the capability of machine learning for estimating the white space availability based on a dataset from a spectrum survey from 170 MHz to 1 GHz. In addition, we present an algorithm for minimizing the effect of hidden nodes on wrongful spectrum allocation and interference. Our optimization algorithm based on supervised machine learning allows increasing the spectrum utilization efficiency with a factor 5 (from 0.09 to 0.47) in the surveyed region. In addition, our algorithm allows decreasing the interference probability caused by the effect of hidden nodes by a factor 6, compared to the traditional distributed allocation of spectrum in Dynamic Spectrum Access networks.

*Corresponding author

Email address: `rodney.martinezalonso@ugent.be` (Rodney Martinez Alonso)

Keywords: Dynamic Spectrum Access, Cognitive Radio, Spectrum Survey, Spectrum Efficiency, White Spaces, Hidden Nodes, Machine Learning.

1. Introduction

The traditional fixed allocation of the spectrum has become a bottleneck for the efficient deployment of new wireless technologies. Spectrum surveys conducted worldwide demonstrate that the global efficiency of the spectrum utilization is lower than 0.25 [1, 2]. For a future all-connected Digital Economy, this inefficient use of the spectrum is not sustainable. In this context, Dynamic Spectrum Access (DSA) networks allow the opportunistic access of unused or under-utilized spectrum in a certain area or instant of time [3]. By exploiting the licensed but unused spectrum or better distributing the spectrum based on the services' dynamic demand, a higher spectrum efficiency could be achieved.

The advances in cognitive radio technologies and smart networks have been fundamental for the development of DSA networks. Besides the pioneering and leading of TV White Space (TVWS) technologies (e.g., IEEE 802.11af [4] and IEEE 802.22b [5]) for the deployment of Wireless Regional Area Networks, cognitive networks have also emerged as a technological solution for more efficient use of spectrum in the mobile cell infrastructure. For instance, Ericsson has introduced a cognitive spectrum sharing technology for dynamically distributing the spectrum between 4G and 5G devices as a function of the throughput demand and users density, as well as dynamically allocating more spectrum for carrier aggregation [6]. However, the DSA is only performed for the domain of a single network operator and for splitting the spectrum bandwidth as a function of the throughput demand between 4G and 5G users. A coordinated spectrum management system for 5G networks is presented in [7]. Although the resource fairness index (as a metric of spectrum efficiency) is increased up to 0.47 for the ISM band, the study in [7], requires a major modification in the 5G infrastructure where a Spectrum Sharing Manager (SSM) retrieves the signaling data and allocates the spectrum for multiple operators. In [8], a deep-

reinforcement learning algorithm for the allocation of spectrum is investigated for a simple ALOHA (from the original acronym of Additive Links On-line Hawaii Area) access mechanism where sensing and collision avoidance is not
30 required. Nevertheless, as fully cognitive radio devices rely on the sensed data by the end-devices, the concept of hidden nodes plays a key role on interference, forming a critical scientific gap in this area.

In DSA networks, hidden nodes are end-devices for which a group of nearby
35 transmitters are not visible and report to their Base Stations (BS) inaccurate data regarding the spectrum utilization. This effect is caused by shadowing and temporal fading in a complex heterogeneous network scenario. It will likely lead to a wrong spectrum assignment and a higher interference [9, 10]. For minimizing the effect of hidden nodes, different cooperative spectrum sensing
40 mechanisms have been proposed in the literature [11, 12, 13, 14, 15, 16]. Compared to these works the main novelty of our research is that our cooperative spectrum sensing algorithm is based on the correlation, pattern finding and inference by Machine Learning of the *spectrum footprints* (i.e., spectrum vectors defined by the signal levels as a function of the surveyed frequencies from
45 multiple geolocations) rather than the perceived signal levels on a per-channel basis. **This means that besides the spatial correlation, our method will also account for the self-correlation in the frequency domain.** Our hypothesis is that a multichannel based inference allows better identifying the information from hidden nodes regarding the cluster spectral footprint, mini-
50 mizing the interference in comparison to traditional algorithms.

The concrete contributions of this paper are as follows. First, based on the nearest neighbors reported data, our algorithm allows inferring the signal level and spectrum utilization patterns across the entire evaluated spectrum. Second, our machine learning based algorithm allows estimating the spectral utilization
55 in locations where no sensing data is available. This is a critical gap for traditional algorithms and it is particularly relevant for IEEE 802.11af devices without sensing capability, as the geolocation databases could be updated in "real-time" from a limited amount of sensors. Third, the algorithm is validated

experimentally using a dataset that we obtained from a spectrum survey: the
60 performance is evaluated and it is shown that the spectrum utilization efficiency
increases and that we reduce the interference probability caused by the effect of
hidden nodes.

The outline of this paper is as follows. In Section 2 we present the state-of-
the-art. In Section 3 we briefly describe the dataset from the spectrum survey,
65 the machine learning algorithm, and the method for spectrum utilization opti-
mization and for minimizing the harmful effect of hidden nodes. In Section 4
we present our research findings. Finally, the research conclusions and future
work are presented in Section 5.

2. State-of-the-Art

70 2.1. Coexistence and Optimization

Guaranteeing the coexistence between the different services dynamically
sharing the same spectrum is a critical requirement for cognitive radio technolo-
gies [17]. Fair access and an environment free of harmful interference should
be guaranteed for all services [18]. Besides the considerations for the use of
75 the spectrum by dynamic spectrum access networks on a secondary basis, the
coexistence between different DSA networks in the same band is not always
achieved. For instance, in an uncoordinated, not cooperative framework, the
coexistence between IEEE 802.22 and IEEE 802.11af is limited, as the first
one will tend to allocate more bandwidth and better-quality spectrum [19].
80 The quantization of spectrum occupancy, interference maps, and geo-location
databases also contribute to avoiding harmful interference. Some technologies
like IEEE 802.11af might fully rely on spectrum geo-location databases from
spectrum survey data. Although geolocation databases allow reducing the re-
ceiver complexity and price, this comes at the cost of a lower spectrum uti-
85 lization efficiency as the databases are not updated in real-time. In [1], authors
investigated different interpolation and occupancy estimation techniques for the

creation of interference and spectrum occupancy maps from spectrum surveys that could improve geolocation database quality.

Most research has focused on optimizing resource allocation, i.e., spectrum
90 and power. For instance, in [3], the authors investigated a reinforcement learning
algorithm for joint collaborative spectrum allocation and a rate-less erasure cod-
ing optimization with the aim of improving spectrum allocation and interference
mitigation. This coding seems to be particularly robust for dynamic spectrum
access where the interference conditions change dynamically as a function of
95 the spectrum allocation by the core controller [3]. However, the authors did
not define a specific spectrum sensing method and assumed an idealistic false
allocation and false-detection probability. In [2] we proposed a multi-objective
optimization algorithm for spectrum utilization efficiency, power consumption,
and radiation of cognitive radio networks by means of a Pareto optimality in-
100 vestigation. The method is intended for a cloud-based access controller and not
for distributed networks, as it requires assessing the signaling and sensed data
from all network devices.

The optimization of the spectrum allocation either for distributed or cloud-
centric architectures relies on the accuracy of the sensing information provided
105 by the eNodes (3GPP-compliant implementation of a BS) and end-devices. For
this reason, the sensing accuracy and channel occupancy estimation are fun-
damental. Indeed, a key challenge in cognitive radio-based networks is the
sensing accuracy in both the spatial and temporal domain. For the temporal
domain, a key performance indicator is the optimization of the sensing time.
110 For this, a trade-off between the throughput and interference mitigation must
be assessed [20]. In [21], the authors present a dynamic adaptive sampling
of the spectrum based on a sequential Monte Carlo method for maximizing
the datarate and improving the channel estimation accuracy. For wideband
sensing, the sampling rate and network idle period for sensing have a major
115 impact on the Quality of Service (QoS), because of the increased sensing time
and noise floor. A compressed sequential wideband sensing for dynamically
finding the number of samples required to estimate the channel occupancy is

presented in [22]. This approach might be feasible for TVWS networks with a lower dynamic variation of the transmission environment. However, for a mobile scenario, the accuracy might be limited. Although traditional Cognitive Radio networks use a listen-before-talk mechanism for scheduling sensing periods and data transmission periods [5, 23], recent research proposes a joint sensing and transmitting cycle [24]. In [24] authors investigated a simultaneous sensing-transmitting cycle using a dual antenna system and signal cancellation for reducing the self-interference caused by the transmitter.

Different research have studied the use of reinforcement learning algorithm for dynamic spectrum access, and in particular Q-Learning [25, 26, 27]. The use of reinforcement learning allows adapting the algorithm to changing environmental propagation conditions and spectrum utilization variations. Notice that clustering is a non deterministic problem. Therefore, the computational complexity of machine learning increase exponentially with the degrees of freedom. For improving the algorithms computational performance further advancements have been done combining supervised learning for Deep Neural Networks and Reinforcement Learning like Deep Q-Learning [28] and also on mixed algorithms like Genetic Algorithms with supervised machine learning [29]. Although, a higher accuracy and adaptability to different environment and scenarios is achieved, it still comes at a significant computational cost that might not be effective for some use cases considering the current state of the art regarding Edge Tensor Processing Unit [30, 31, 32]. This is particularly relevant for applications where cost and energy efficiency are key performance indicators. This is the case of our intended application for Dynamic Spectrum Access in remote and rural scenarios where it is required a better balance between the computational capacity at the edge and the front-haul efficiency. Therefore, in this paper we focus on 1D neural networks aiming to maximize the outcomes of supervised learning algorithms in terms of improving the trade-off between accuracy, adaptability and computational complexity.

Despite the advances in sensing and occupancy estimation, state-of-the-art spectrum allocation optimization relies on the accuracy of the signalization in-

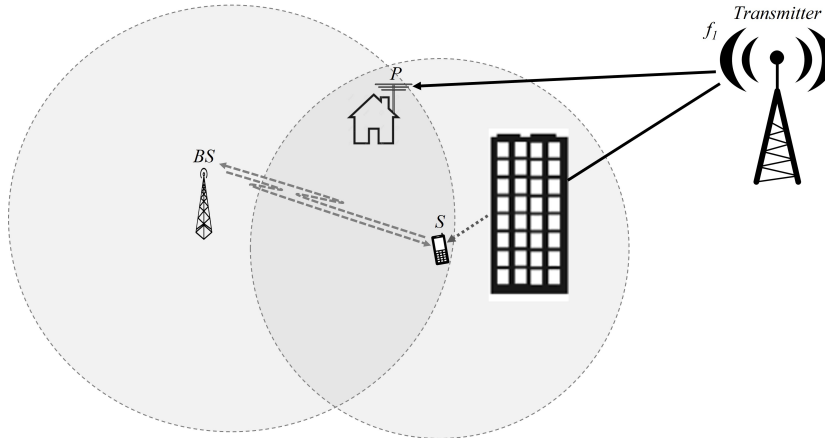


Figure 1: Interference caused by Hidden Nodes in the context of Dynamic Spectrum Access networks. *BS*: Base Station; *P*: Primary service receiver; *S*: Secondary service device (enabled with cognitive radio functionalities).

formation provided by the end-devices. Due to shadowing and fading, a protection margin should be considered for most of these methods [9]. In addition, the hidden nodes in the context of dynamic spectrum access networks have a significant effect on interference and the coexistence of heterogeneous networks [10].

2.2. Cooperative Spectrum Sensing and Hidden Nodes

Fig. 1 shows a diagram describing the hidden nodes problem in the context of Dynamic Spectrum Access networks, specifically for a TVWS network sharing the spectrum with broadcasting services.

A secondary spectrum user *S* is located behind an obstacle in the direction of the primary service transmitter. The signal level detected by *S* leads to a wrong detection of f_1 as white space (spectrum available for reuse by the wireless network). As a consequence, the nearby primary licensed user *P* (broadcasting receiver) experiences harmful interference due to the wireless communication between *S* and the *BS* operating in f_1 [9].

Although for other problems related to geo-tagged variables, interpolation methods like Delaunay and Kriging might provide a good approximation between the correlation of the geospatial data and the target objective [33], it is

not the case of spectrum data. By one hand spectrum data is not only correlated to the spatial geolocation but to the frequency domain (i.e, self-correlation across the frequency domain). Indeed, traditional geospatial interpolation methods performs poorly when the target objective is affected by a third variable.

170 By other hands, without cooperative spectrum analysis (i.e, fingerprinting spectrum multicorrelation in our application), it is not possible to discard the data from unreliable nodes. For tackling the hidden node problem, collaborative spectrum sensing algorithms allow leveraging the spatial diversity from multiple sensors in cognitive radio networks. For instance, [12] presents an optimized

175 algorithm for cooperative spectrum sensing which reduces the number of sensing devices required for reaching a certain occupancy error threshold. However, it is assumed that the distance between sensing devices is small compared to the distance from the primary transmitters. This is reliable for TVWS networks with a predominant High Tower High Power architecture in the primary network.

180 For a more complex heterogeneous scenario, which contains different network architectures including Low Power Low Tower infrastructure, small end-device transmitters and a significant variance of radiated power, a per-channel based estimation only might not be accurate. This due to the fact that the distance for which an acceptable correlation is achieved, dynamically varies as a function

185 of time and frequency in a realistic heterogeneous network scenario. Also [13] presents a cloud-based algorithm for estimating a channel occupancy based on energy detection and the power spatial variance on a channel-per-channel basis. In [14] authors present a machine learning based algorithm for classifying measurement vectors from multiple sensors into empty or occupied channel categories.

190 However, the vectors for correlating multiple locations are conformed from measurements in the time domain only. A pure heuristic algorithm where the cognitive radio devices are grouped for sensing different channels in a time schedule is proposed in [16]. Although this algorithm optimizes the sensing time and maximizes the channel throughput, a whole instantaneous picture of the spectrum utilization at each cluster is never found. In [11] authors present

195 a Social Internet of Things (SIoT) based architecture for optimizing spectrum

allocation and minimizing the interference probability. This concept inspired by human social networks allows that multiple devices exchange spectrum utilization information regardless of their cognitive radio capability. This means that devices from heterogeneous networks collaborate on the sensing even when they do not use that information for spectrum allocation. Different machine learning algorithms including deep learning and reinforcement learning are proposed in [27] for the context of cooperative spectrum sensing in dynamic spectrum access networks for 5G. Nevertheless, further research is required for investigating the effect of hidden nodes in the system accuracy and performance, particularly for reinforcement learning when the reward function does not discard data from unreliable nodes.

Most studies approach the spectrum occupancy and hidden node problem from an individual channel perspective, i.e., independently correlating each channel level vector. In a High Power High Tower infrastructure (e.g., broadcasting service as a primary spectrum user) this will likely lead to a lower spectrum over-allocation (false alarm). However, in more complex scenarios where multiple and heterogeneous networks coexist, a whole correlation of the signal levels as a function of frequency and geo-location (*spectrum footprint*) might lead to a higher spectrum utilization efficiency with a lower interference. In general, a gap in the state of the art is the lack of a multi-channel correlation approach between the spatial domain and self-correlation in the frequency domain. Nevertheless, a method for estimating a multiband radio environmental map by a deep learning completion autoencoder is presented for the first time in [45]. This method outperformed most traditional interpolation methods in terms of accuracy and computational efficiency. The deep learning architecture proposed in [45] comprises several layers where the number of neurons depends (among others) on the number of sampled frequencies. As a comparison, our proposed machine learning algorithm comprises a single hidden layer of 228 to 402 neurons (see $N_{neurons}$, in Fig. 3), depending on the sub-band of interest and setup. For the multi-frequency spectrum occupancy estimation, our correlation-based pre-clustering and machine learning algorithms allow achieving a similar

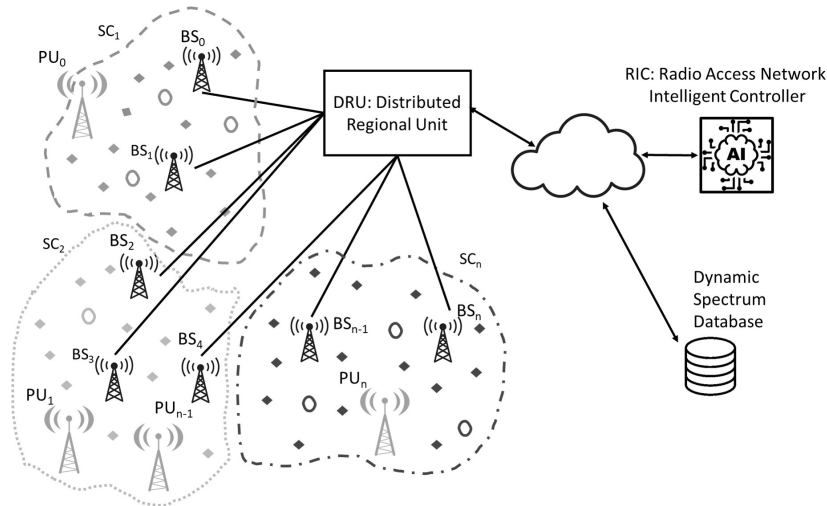


Figure 2: System Level Conceptual Overview of the Dynamic Spectrum Access Network. *PU*: Primary User, defines the service with the primary license of the spectrum, *BS*: Cognitive Radio base stations, as secondary unlicensed users of the spectrum, *SC*: Organization of the network in spatial spectrum clusters, *Diamond Markers*: cognitive radio user devices or sensors, *Circle Markers*: user devices without fully-compliant cognitive radio functionalities, *DRU*: Distributed Regional Units, *RIC*: Cloud-centric Regional Access Network Controller

accuracy and a higher computational efficiency than state-of-the-art methods. A quantitative analysis is presented in Sub-Section 4.5.

230 3. Method

By contrary to the traditional fully distributed cognitive radio networks, at a high system level we base our method on a hybrid network architecture (i.e., control functions can be performed either at the edge, distributed regional units, cloud-centric or mixed). Fig. 2 shows a conceptual overview of the dynamic spectrum access networks at a high system level.

This architecture resembles the O-RAN (Open Radio Access Network) architecture for cell-free networks. In this paper we do not investigate cell-free radio resource allocation with multiple antennas per user, but cell-centric infrastructure where the network is dynamically organized in terms of spectrum resources.

240 In addition, our proposed high-level architecture for dynamic spectrum access
 offers a high flexibility in terms of the distribution of the computational pro-
 cessing. The spectrum geolocation databases (e.g., IEEE 802.11af [4]) allow
 reducing the complexity of the end-devices (i.e., circle markers in Fig. 2). How-
 ever, a major disadvantage of the geolocation databases is that they rely on
 245 costly spectrum surveys and are difficult to keep updated. To overcome this,
 our system level proposal allows dynamically updating the information of the
 databases from the information retrieved by fully compliant cognitive radio de-
 vices or distributed sensors (i.e., diamond markers in Fig. 2). As demonstrated
 in [2] a cloud-centric architecture outperforms the traditional distributed cogni-
 250 tive radio networks in terms of spectrum utilization efficiency, but at a cost of
 increased computational complexity and front-haul overload. In the proposed
 system level architecture, the radio resource allocation is distributed between
 the *DRU* and the *RIC*. The *DRU* will be in charge of the regional sensing cycles,
 data pre-processing and clustering (*SC* in Fig. 2). The *RIC* will perform the fi-
 255 nal allocation of the radio resources (i.e., spectrum allocation) and maintenance
 of the Dynamic Spectrum Geolocation Database.

Our proposed method for optimizing the spectrum allocation is based on a
 mixed clustering and machine learning algorithm. Although the architecture
 presented before is quite dynamic and flexible, we assume the clustering part is
 260 performed by the *DRU* and the final allocation of the spectrum and spectrum
 database management is performed at the *RIC*.

Fig. 3 shows the general rationale of our proposed approach as a flow chart.
 The main goal is to infer the signal levels (L) as a function of the frequency (f)
 and geolocation ($GPSx;GPSy$) at any given location u_i in the evaluated area
 265 (circular marker in Fig. 3), considering the measured data at a limited number
 of locations (diamond markers s_1, s_2, \dots, s_n in Fig. 3) in the sub-1 GHz bands.
 In the context of machine learning the inference is the capability of estimat-
 ing new output data based on a limited number of inputs and labeled output
 samples. Based on the correlation between the data from different locations,
 270 data clusters are created (e.g., at the *DRU* level from Fig. 2) for decreasing

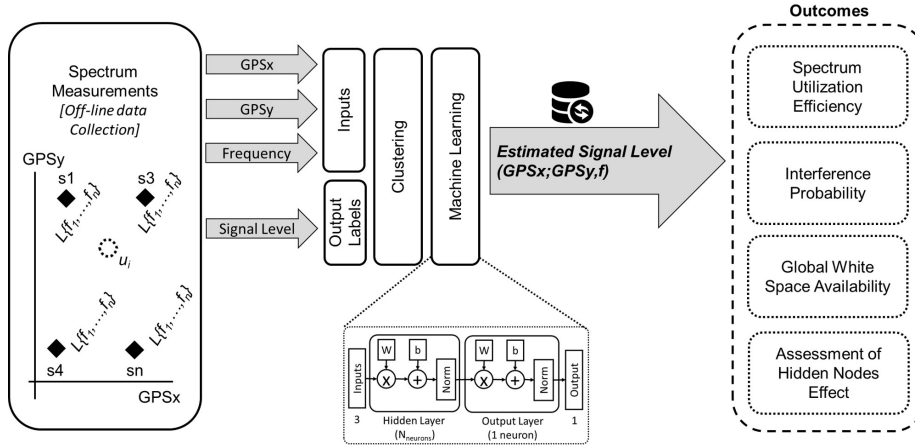


Figure 3: Rationale. *Diamond markers: measured locations; u_i marker: Unknown spectrum information; $GPSx$: Longitude [$^\circ$]; $GPSy$: Latitude [$^\circ$]; f : Frequency; L : Signal level.*

the machine learning computational requirements (e.g., at the *RIC* level from Fig. 2). Based on the machine learning output, the spectrum utilization efficiency, interference probability, and global white space availability can also be estimated. The predicted signal levels and spectrum occupancy estimations could be used for updating in "real-time" a geolocation database for dynamic spectrum access networks (see Dynamic Geolocation Database in Fig. 2). We also assess the effect that hidden nodes reporting inaccurate data might have in the machine learning inferred function. Further details are provided in the following subsections.

3.1. Spectrum Measurements: Data Collection and Setup

We use a dataset from a spectrum survey performed in a rural environment at the outskirts of Havana, Cuba (border between Havana, Mayabeque and Artemisa provinces). The dataset consists of signal level measurements from 84 surveyed locations from 170 MHz to 1 GHz, with a frequency resolution of 1.48 MHz. The signal level measurements are based on energy detection and where automatically performed by the enhanced spectrogram function from a

spectrum analyzer i.e., spectrum of frequencies of a signal as it varies with time. The measurements were performed at the peak fading times (maximum fading lower than 5 dB) without time coherence. For compensating the lack of exact
 290 temporal coherence in the time domain we account for near-maximum signal levels (99th percentile). Therefore, the total dataset size is 47,040 signal level (99th percentile) samples (i.e., matrix of 84 locations by 560 sampled frequencies) considering the signal levels for the 99th-percentile in the time domain during a period of half-hour. Fig. 4 shows the surveyed area. The diamond
 295 markers correspond to the measurement locations distributed in a grid of points separated by approximately 1 km. More details on the measurement setup can be found in [34].

3.1.1. Data Classification for Clustering

For finding a pattern in the signal level as a function of frequency from dif-
 300 ferent locations, we first perform a classification of the dataset. The data is classified in sub-clusters depending on the correlation of the signal level vectors (i.e., vector of the signal levels as a function of the frequency at a certain location, which we define as the *spectrum footprint*). Algorithm 1 details a pseudo code of the algorithm for finding the correlation of the spectrum vectors for
 305 each possible combination of locations. This algorithm can be independently implemented in the *DRU* proposed in the system level architecture from Fig. 2.

Our aim is to determine the maximum cluster diameter (d_{max}) for which a correlation higher than 0.5 is achieved with a probability equal or higher than 0.9 (10th-percentile). In this way, if the signal level correlation between a location
 310 and their neighbors is outside the 10th-percentile correlation within its cluster we assume this location might be a hidden node.

First, we calculate the distances between each location and all their neighboring locations by means of the *harvesine* equation (see Equation 1) and further we correlate the signal level vectors from each location with their neighbors (Al-
 315 gorithm 1 line 2 to 7). Here, Cr_{ij} and dx_{ij} are two linked 2D-matrices containing all the possible correlations between locations for any given distance between

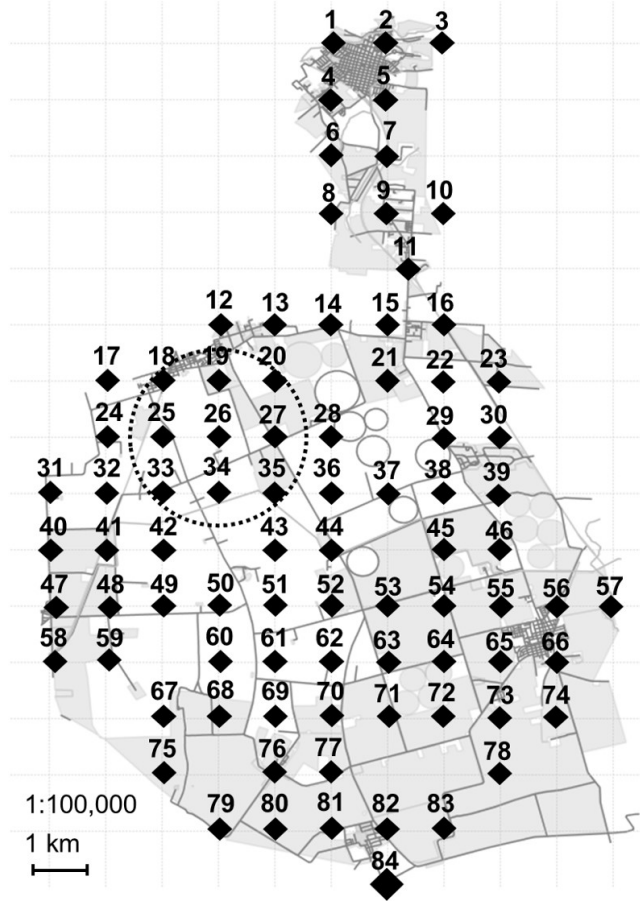


Figure 4: Spectrum Survey Map. *Diamond markers: measurement locations.*

them.

The *haversine* equation for calculating the distance between any given geolocation i and j is defined as:

$$dx_{ij} = 6371 \cdot 2 \cdot \operatorname{atan}^2(\sqrt{a}, \sqrt{1-a}) \quad (1)$$

Algorithm 1 Data Classification for Clustering

Inputs: Lv (Signal Levels)[dBm], $GPSx[]$, $GPSy[]$, $Freq[MHz]$
Output: $Cr[]$, $dx[]$, d_{Cr} , d_{max}

```

1:  $N_p$ : number of locations
2: for  $i=1:(N_p-1)$ 
3:   for  $j=(i+1):N_p$ 
4:      $Cr_{ij} = \text{Correlation}(Lv_i, Lv_j)$ ;
5:      $dx_{ij} = \text{Haversine}(GPSx_i, GPSy_i, GPSx_j, GPSy_j)$ 
6:   end for;
7: end for;
8: for  $d_{ref} = 0.5:5$ 
9:    $d_{Cr}[] = \text{percentile}(Cr\{d_{ref}\}, 10)$ 
10: end for;
11:  $d_{max} = \max(d_{Cr}) \forall Cr \geq 0.5$ 

```

320 where a is calculated as:

$$\begin{aligned}
 a = \sin^2 \left[\frac{\pi}{360} \cdot (GPSy_j - GPSy_i) \right] + \cos(GPSy_i) \cdot \\
 \cos(GPSy_j) \cdot \sin^2 \left[\frac{\pi}{360} \cdot (GPSx_j - GPSx_i) \right]
 \end{aligned} \tag{2}$$

The correlation between spectrum vector of signal levels Lv as the function of frequency for any given location i and j is defined as:

$$\rho(Lv_i, Lv_j) = \frac{\mathbb{E} [(Lv_i - \mu_{Lv_i}) \cdot (Lv_j - \mu_{Lv_j})]}{\sigma_{Lv_i} \cdot \sigma_{Lv_j}} \tag{3}$$

325 where \mathbb{E} is the expectancy (weighted mean), μ is the mean, and σ_{Lv} is the standard deviation. In this way the correlation is not referred to the deviation of the mean but a weighted mean where a group of values might be more representative (higher weight) than others in the vector.

330 Finally we find for different cluster diameters d_{ref} the worst achievable correlation (10^{th} percentile) considering all the possible clustering combinations (lines 8 to 10 in Algorithm 1). Then the spectrum data can be further classified in sub-clusters that include the neighboring locations up to d_{max} . Therefore, d_{max} corresponds to the highest cluster diameter for which a correlation higher

than 0.5 can be achieved. In this paper we will investigate the performance of a machine learning algorithm for the worst case cluster found in our dataset (lowest correlation) considering a cluster size d_{max} . The area delimited by the dashed line in Fig. 4 corresponds to the worst-case cluster in terms correlation
335 between the signal level vectors. This classification allows saving in computational time and finding patterns in spectrum utilization.

3.2. Inference of Spectrum Footprints by Machine Learning

The machine learning will allow to learn the spectrum utilization patterns for optimizing the Dynamic Spectrum Access of network devices. In particular,
340 machine learning might enhance the network resource allocation (i.e., spectrum allocation) by learning from the real-time propagation conditions and spectrum utilization [35]. In addition, the algorithm should recognize a possible hidden node and minimize the corresponding harmful interference effect through data
345 classification and pattern recognition.

For our experimental evaluation, we consider supervised learning, i.e., the algorithm works with labeled data, where both the input data and corresponding output data are known to the system [35]. In this context, the goal of supervised learning is finding the pattern between the input and output data or predicting
350 the behavioral function for unknown geolocations for any given frequency within the evaluated area (i.e., predicted signal levels for further estimating the white space availability and calculating the spectrum utilization efficiency).

Defining the appropriate training method for the intended application is a complex problem that depends on several variables, e.g., problem complexity,
355 the number of data samples in the training and validation set, the number of weights, biases and hidden neurons in the network, the error goal, and whether the network is being used for pattern recognition (discriminant analysis) or function approximation (regression). For this reason, we empirically evaluate the performance, error, and convergence of different 1D Neural Network inferred
360 functions for estimating the target objective.

The local minima of the signal levels defines the final allocation of the available spectrum (white spaces). More details on the threshold considered are provided in following subsections. We hypothesize that machine learning methods implemented for function fitting by finding local minima for both the spatial and frequency domain will have a better performance in our application. This is because, not finding the local minima of the signal level as a function of geolocation and frequency will lead to an over-allocation of spectrum and higher interference. The drawback of these kinds of methods is that the global minimum of the function might not be found. However, not finding the global minimum will lead to a lower interference than overestimating the real white space availability for most geo-locations and frequencies (local minima). This means better results should be obtained from methods oriented to progressively finding the function's local minima.

Least-squares fitting methods are parameterized mathematical models for finding a set of data points by minimizing an objective (variable) expressed as the sum of the squares of the errors between the model function and a set of data points [36]. The following methods are used for the 1D neural network training: Broyden–Fletcher–Goldfarb–Shanno (Quasi-Newton) [37], Levenberg-Marquardt [36], Resilient Backpropagation [38], and Variable Learning Rate Backpropagation [39, 40].

3.3. Machine Learning based Algorithm for Inferring the Signal Levels at any Location

Algorithm 2 shows the machine learning algorithm for predicting the signal level as a function of the geo-location coordinates and frequency in the evaluated scenarios. This algorithm is based on k-cross validation for validating the fitting weights of the neural network. The performance of the different training methods for the neural network were empirically evaluated using the same algorithm. We assume this algorithm runs in the RIC from the architecture proposed in Fig. 2. This is for guaranteeing the coherence of the dynamic spectrum database from multiple nearby DRU's in future applications. However, in

Algorithm 2 Machine Learning Algorithm for Predicting the Signal Level Distribution

Inputs: $GPSx$ [$^{\circ}$], $GPSy$ [$^{\circ}$], $Freq$ [MHz]

Output: L (Signal Level) [dBm]

- 1: $N_{samples}$: Number of samples in the sub-cluster
- 2: $N_{neurons}$: Number of neurons
- 3: k : k-fold partition of the population
- 4: $[GPSx_n, GPSy_n, Freq_n, L_n] = \mathbf{Normalize} (GPSx, GPSy, Freq, L)$
- 5: **for** $Sim_x = 1 : Max_Sim$
- 6: **net** = feedforwardnet ($N_{neurons}$, 'training_method');
- 7: net_estimator = neuralnet (net);
- 8: **Partition** $_k = \mathbf{cvpartition} (N_{samples}$, 'kfold', k);
- 9: **for** $i=1:k$
- 10: find (**training** (**Partition** $_k, i$));
- 11: find (**validation** (**Partition** $_k, i$));
- 12: **Data_training** { i }
- 13: **Data_validation** { i }
- 14: **end for**;
- 15: **for** $i=1:k$
- 16: **net** = **train**(**Data_training** { i }[($GPSx_n, GPSy_n, Freq_n$);(L_n)]
- 17: **net_Output**{ i }= **net** (**Data_validation** { i }($GPSx_n, GPSy_n, Freq_n$))
- 18: ML_error{ i } = |net_Output{ i }- L_n { i }|;
- 19: **end for**;
- 20: **Linferred** $_x = \mathbf{normalize}$ (net ([$GPSx_n, GPSy_n, Freq_n$]);
- 21: Error $_x = \mathbf{mean}$ (ML_error)
- 22: STD_PAVE $_x$ (Linferred $_x$)
- 23: **end for**;
- 24: **SUE** (Linferred $_x;L$){ $GPSx, GPSy, Freq$ };
- 25: **Pinterference** (Linferred $_x;L$){ $GPSx, GPSy, Freq$ };

this paper we assume the data proceed from a single DRU.

3.3.1. Inputs and Outputs

The machine learning receives as inputs the center frequency of each spectrum sample ($Freq$) and the geo-location coordinates from the spectrum survey locations, i.e., $GPSx$: Longitude [$^{\circ}$] and $GPSy$: Latitude [$^{\circ}$]. The output in

395

Algorithm 2 corresponds to the Signal Level at $(GPSx;GPSy;Freq)$ from the spectrum surveyed locations. The input and output data are normalized for avoiding inputs having unfair contribution to the weight fitting by the learning method (line 4 in Algorithm 2). In this way the general normalized learning rule for any method will be defined in terms of the neuron weights variation between iterations as:

$$\Delta\omega = (O - O') \cdot \frac{I^T}{\|I\|} \quad (4)$$

where $\Delta\omega$ is the differential weight matrix between iterations, O is the target labeled output, O' is the neuron response, and I is the input matrix.

3.3.2. Definition of the Neural Network Main Hyperparameters

The main hyperparameters of the neural network are the number of neurons and the k-fold partitioning. The number of hidden neurons in the 1D Neural Network is denoted by $N_{neurons}$ (line 2 in Algorithm 2). The upper limit of $N_{neurons}$ that does not result in over-fitting is defined as follows:

$$N_{neurons} \leq N_{samples} \cdot [\alpha \cdot (N_i + N_o)] \quad (5)$$

where $N_{samples}$ is the number of samples in the spectrum survey dataset (line 1 in Algorithm 2), α is a scaling factor for setting the ratio between hidden neurons, the total number of samples, the number of input (N_i) and outputs (N_o) layers. The ratio of training and validation samples is defined by the hyperparameter k (line 3 in Algorithm 2). As the data partitioning has a significant impact in the trade-off between accuracy and computational complexity, more details on k -fold will provided in the following subsections. Indeed, we iterate the algorithm for different combinations of the machine learning hyperparameters (k and α) in order to fine tuning the algorithm. For benchmarking the hyperparameters we consider as cost parameters the mean error [dB] and training time [s].

3.3.3. Number of Simulations

420 For determining if the machine learning solution is not over-fitted, is coherent and reproducible across multiple replications, we introduce a heuristic algorithm to assess the machine learning performance. For this reason, the algorithm runs for a total number of simulations (Max_Sim in line 5, Algorithm 2). The number of simulations is defined by the Progressive Average (PAVE) of the machine learning objective parameter (i.e., Signal Level). We consider that 425 if the progressive average of the signal level has a standard deviation higher than 2 dB, the number of simulations Max_Rep is not high enough or that the combination of the machine learning hyperparameters does not provide a convergent solution (i.e., not reproducible across multiple realizations). The progressive average of the objective function is computed after each replication 430 of the machine learning model for each simulation (line 22 in Algorithm 2).

3.3.4. Neural Network Structure and Data partitioning

The structure of the 1D Neural Network for the training method defined by *training_method* is then defined, consisting of an input layer, a subsequent connection between each hidden neuron and the output layer. A neural estimator 435 (*net_estimator*) from the MATLAB Deep Learning Toolbox is created based on the defined structure (lines 6 and 7 in Algorithm 2).

For training and further validating the performance of the machine learning methods investigated (from Section 3.2), and solving the fitting function and pattern recognition problem, the spectrum survey dataset is divided into 440 a *training* and *validation* subset. For the neural network assessment we only evaluate the worst-case subcluster retrieved from Algorithm 1. We use the k-fold cross-validation for randomly splitting and distributing the samples for each subset. For k iterations, $k - 1$ folds are assigned to the training subset, and the remaining one is used as the validation subset (Line 9 to 14 in Algorithm 2). 445 We evaluate the performance of the machine learning methods in Section 3.2 considering different values of the k-fold and training to validation subset ratios, i.e, $k = 2(50 : 50)$, $k = 3(70 : 30)$, $k = 5(80 : 20)$, and $k = 10(90 : 10)$.

Although the computational performance of k cross-validation is not the
450 highest, this method achieves an acceptable trade-off between the number of
samples required for validation, accuracy, and avoiding over-fitting. A major
drawback with k cross-validation is that the method variance might be signif-
icantly high. This means that different replications of the machine learning
might lead to solutions with a high standard deviation of the objective func-
455 tion. For avoiding this, we investigate the convergence of the machine learning
algorithm, by performing multiple replications of the algorithm and analyzing
PAVE. For any given configuration of the machine learning hyperparameters
(including k), we consider that the algorithm converge if the PAVE has a low
standard deviation (as defined in Sub-Section 3.3.3) [41].

460 3.3.5. Machine Learning Training and Validation

The Neural Network is trained and validated for each k -fold combination
(line 15 to 19 in Algorithm 2). Nevertheless, for avoiding under-fitting each
batch of data subsets is passed through the training algorithm several times
(*Epoch*). The maximum *Epoch* number is set to 250 and the under-fitting con-
465 dition is controlled by the machine learning mean square error. We have found
that for our dataset for an *Epoch* range between 100 and 250 there is not a
significant variation of the machine learning performance.

After each replication of the machine learning algorithm defined by *Max_Rep*
a matrix of the objective parameters (*Linferred_x*: Inferred Signal Levels) is
470 built. The mean error is also calculated considering each inferred value (i.e.,
Error_x) (line 20 to 21 in Algorithm 2). After all the simulations, the the rel-
ative Spectrum Utilization Efficiency and Interference probability is calculated
based on the *Linferred_x* matrix and the original output data (line 24 and 25 in
Algorithm 2). The details of the functions for quantifying the Spectrum Utiliza-
475 tion Efficiency and Interference Probability are provided in the next subsection.

3.3.6. Quantifying Spectrum Utilization Efficiency and Interference Probability

ITU-R-SM.1046-2/2006 [42] provides general criteria for the evaluation of spectrum utilization factor and spectrum efficiency. A relative Spectrum Utilization Efficiency can be determined as the ratio of the Spectrum Utility achieved by two Dynamic Spectrum Access systems. The Spectrum Utility is equivalent to the white spaces that are useful for providing a secondary service under a DSA network (available at least 99% of the time). We consider a certain portion of spectrum is a White Space and can be allocated to a communication service if the signal level is below -95 dBm during 99% of the time. This level is based on previous works for TVWS [2], considerations of interference maps from [1], and also considers the maximum allowable interference at a distance of 3 times the cell radius (edge of next cell reusing the same frequency) for the case of the sub-bands dedicated mainly to mobile services [43].

For comparing our solution we consider as reference the traditional distributed spectrum allocation by a DSA network in the UHF band at any given location. In the traditional cognitive radio network the spectrum availability in a certain location is defined by a *single sensor* (measurement from a single location). For the spectrum allocation decision by our algorithm (and for calculating the Spectrum Utility) we consider that the spectrum is detected as available by the *majority of the sensors* (signal level below the decision threshold in more than 50% of the locations). The relative Spectrum Utilization Efficiency is then calculated as the ratio between the Spectrum Utility that is achieved by a standard distributed DSA system SU_{std} and the Estimated Spectrum Utility by the machine learning SU_{ml} (in Equation 6).

$$SUE_{ml} = \eta_{max} \frac{SU_{ml}}{SU_{std}} \quad (6)$$

where η_{max} is the maximum spectrum utilization factor that can be achieved discarding the spectrum that is actually assigned and in use at any given location and instant of time.

The interference probability P_{Iml} is calculated as the ratio between the num-

ber of frequency samples (independent inputs N_f) and the number of times
 505 (N_{Iml}) the machine learning level estimation is below the threshold of -95 dBm
 (spectrum detected as available) while the output (spectrum survey data at
 any location within the evaluated subcluster) is above such level (spectrum not
 actually available), leading to a spectrum over-allocation and a probable inter-
 ference to the primary service. Equation 7 defines the interference probability
 510 of the machine learning estimation.

$$P_{Iml} = \frac{N_{Iml}}{N_f} \quad (7)$$

3.4. Global White Space Availability Estimation

Beside the sub-cluster based approach (in Section 3.1.1), we also evaluate
 the performance of a simplified version of the machine learning algorithm for
 estimating the global white spaces availability in the whole area. This is per-
 515 formed for statistical purposes as it can be informative for regulators regarding
 the quantification of spectrum occupancy. For the white space availability es-
 timation no data pre-classification from Algorithm 1 is implemented. In this
 case, the white space availability as a function of geolocations is passed to the
 machine learning algorithm as a tagged output (i.e., White Space availability
 520 will be the output in Algorithm 2, instead of the signal levels). The inputs for
 the algorithm will be the geolocation coordinates $GPSx;GPSy$. The white space
 availability is assumed to be computed by each node independently from the
 sensed data at their location using as reference the same occupancy threshold
 of -95 dBm.

525 Therefore, the percentage of white space availability in any given location
 is equivalent to the Spectrum Utility from Equation 6. The white spaces dif-
 ferential prediction (ΔW) at a certain location i is calculated as the difference
 between the estimated by the machine learning (Wp) and maximum white space
 availability accounted for from the spectrum survey measurements (Ws).

$$\Delta W_i = Wp_i - Ws_i \quad (8)$$

530 When the prediction ΔW_i is positive, there might be an over-allocation of the
 spectrum that will potentially lead to interference. When ΔW_i is negative,
 there might be an under-allocation, meaning the interference is reduced but at
 the cost of a lower spectrum utilization efficiency. Taking into account only
 the mean of ΔW might lead to a significant over-allocation or interference in
 535 a certain area. For this reason, an equally balanced weight between the 95th-
 percentile and the mean of ΔW is considered. Although we aim to achieve
 a higher spectrum utilization efficiency, it can not be at the cost of a higher
 interference. The interference probability of having the allocation decision been
 made at the edge is then calculated considering the number of over-allocated
 540 white spaces (Equation 7).

3.5. Assessment of the Interference Caused by Hidden Nodes

The detection of interference signals may not always be reliable, even be-
 tween systems using the same radio access technology, due to the hidden node
 problem [44, 9]. For minimizing the harmful interference caused by hidden
 545 nodes in DSA networks, we propose a learning mechanism, where the spectrum
 allocation takes into account the correlation between the signal level vectors
 of different neighboring locations (i.e., correlation of the *spectrum footprints*)
 within a cluster with a maximum diameter d_{max} . First, the classification pro-
 cess described in Section 3.1.1 is implemented, and the machine learning method
 550 is trained as described in Algorithm 2. The resulting pattern recognized by the
 machine learning will be used as a reference. In a second step, we artificially
 reduce the Signal Level of a random location by the measured shadow variation
 in the area. The machine learning is then trained with these data mimicking
 the worst-case effect caused by a hidden node. We compare the inferred signal
 555 levels by the machine learning with and without the effect of the hidden node.
 In addition we benchmark the machine learning capability to minimize the effect
 of the hidden nodes against the spectrum allocation by a traditional cognitive
 radio network.

The interference probability for the machine learning estimation is calcu-

560 lated in the same way described by Equation 7 considering only the data for the analyzed cluster (sub-area for which a moderate-high correlation is achieved). The mean variation caused by the hidden node in the machine learning estimation is accounted for by means of the difference of the area below the fitting functions for each case:

$$Vm_{hn} = \frac{1}{N_f} \cdot \left[\sum_{f=1}^{N_f} (Lp_f - Lp'_f) \right] \quad (9)$$

565 where Vm_{hn} is the mean relative variation caused by the hidden node in the machine learning signal level estimation, N_f is the number of frequency samples at each location, f is the index corresponding to a certain frequency sample, Lp_f is the signal level estimated by the machine learning without the hidden node effect for f , and Lp'_f is the signal level estimated considering the effect of
570 the hidden node.

3.6. Constraints and Limitations

We observed that the noise floor of the measurement instrument should be at least 10 dB below the decision threshold for allocating the spectrum and determining the white space availability. In our measurements the noise floor was
575 -110 dBm. When the noise floor of the instrument and the spectrum allocation decision threshold is too close, the performance of our algorithm for allocating the spectrum is quite limited without over-fitting (e.g., less than 2% improvement on spectrum utilization efficiency for a noise floor to allocation threshold margin of 5 dB).

580 4. Results

4.1. Correlation as a Function of the Cluster Diameter

Fig. 5 shows the 10th-percentile correlation for different cluster diameters (i.e., the probability of having a higher correlation between two locations within the cluster of diameter d is higher than 0.9) We found that for a maximum

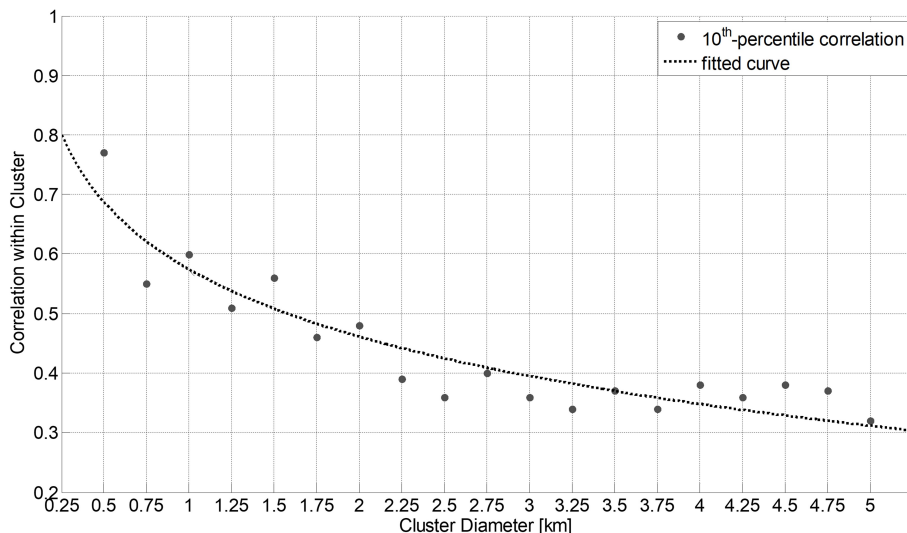


Figure 5: 10th-percentile correlation of the signal level vectors from different locations as a function of the cluster diameter.

585 cluster diameter (d_{Cr}) of 1.6 km there is a spatial correlation between the signal level samples across the measured spectrum higher than 0.5 with a probability of 0.9.

4.2. Machine Learning Estimation of the Signal Levels

We investigated the performance of Algorithm 2 (Section 3.3) for different
 590 machine learning methods. Fig. 6 shows the mean signal levels (for the evaluated sub-cluster in the spatial domain) from the spectrum survey compared to the inferred ones by the machine learning for different training methods, Fig. 6 a) shows the results corresponding to the broadcasting television band segments and Fig. 6 b) the remaining frequencies up to 1 GHz. The inference by the machine learning of the mean signal levels in Fig. 6 correspond to the sub-cluster
 595 having the samples with lower multi-correlation with their neighbors up to d_{Cr} . Therefore, here we show the machine learning worst-case performance for the surveyed area (i.e., see dashed line in Fig. 4). Based on the machine learning inferred signal levels by each method and considering the allocation threshold from

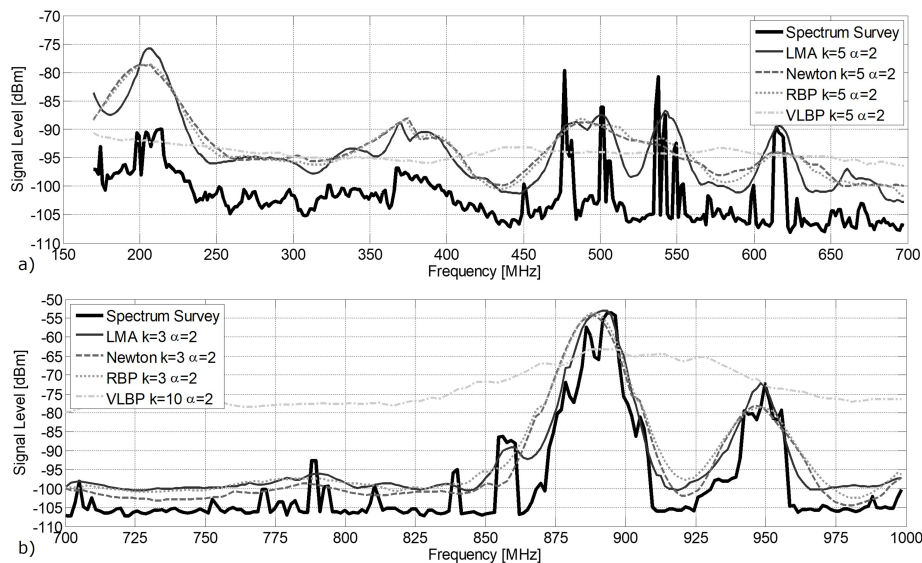


Figure 6: Machine Learning Inference of the Mean Signal Level (spatial mean for 99th-percentile of time) for the worst-case sector, considering a) Broadcasting television spectrum b) Remaining spectrum up to 1 GHz including the mobile band segments, for the training methods *Spectrum Survey*: accounted for from the spectrum survey data, *LMA*: Levenberg-Marquardt, *Newton*: Broyden-Fletcher-Goldfarb-Shanno Quasi-Newton, *RBP*: Resilient Backpropagation, *VLBP*: Variable Learning Rate Backpropagation

600 Section 3.3.6, the SUE is calculated. For the sub-band assigned (mainly) to the broadcasting television as primary service, the best results in terms of SUE are obtained for $k = 5$ and $\alpha = 2$ for all the optimization methods. For Levenberg-Marquardt, as the signal level estimation difference between $k = 5$ and $k = 3$ is barely 0.5 dB the SUE difference is lower than 7%. However, for other methods,

605 the difference is at least 14%, meaning that at least 80% of the samples are generally required for the training process. Levenberg-Marquardt method achieved the best result in terms of Spectrum Utilization Efficiency (see Equation 6), i.e., $SUE = 0.47$. This value is 5 times higher than the current spectrum utilization efficiency in this sub-band ($SUE = 0.09$). The Levenberg-Marquardt method

610 showed a better performance for finding the local minima, and as a consequence
a better curve fitting is obtained. This is because Levenberg-Marquardt method
interpolates the objective function by adaptively varying the fitting parameters
between the Gauss-Newton and the gradient descent methods [36] and generally
a higher fitting accuracy is achieved. However, the computational time of this
615 method is higher than Gauss-Newton and Broyden-Fletcher-Goldfarb-Shanno
Quasi-Newton methods. Although for the Variable Learning Rate Backpropaga-
tion a $SUE = 0.23$ is achieved, the obtained function does not fit the patterns
of the signal variations across the spectrum from the surveyed area. For all
the methods, independently from the achieved SUE the relative interference
620 probability does not increase.

For the sub-band between 700 MHz and 1 GHz (Fig. 6b), with a predom-
inant allocation to mobile communication services, the best machine learning
performance is obtained for $k = 3$. For a higher ratio of training samples the
SUE slightly improves (less than 0.03) but at the cost of a higher variation of
625 the signal level prediction (approximately by 1 dB) and a significantly higher
computational time. For the Variable Rate Learning Backpropagation method
(VLBP in Fig. 6b), independently from the training-validating ratio, a fitting so-
lution is never found. The best spectrum utilization efficiency is again achieved
for the Levenberg-Marquardt method (i.e., $SUE = 0.55$ on average across all
630 simulations). However, the variation of the predicted signal level is 1.4 dB
higher compared to the second-best (BFGS Quasi-Newton). Notice that the
inferred signal levels for the above 700 MHz sub-band are closer to the spec-
trum survey data (in Fig. 6). In the Low-Power Low-Tower configuration of
the mobile infrastructure, a more uniform and consistent radiation footprint
635 is obtained across the surveyed area, compared to the High-Power High-Tower
configuration predominant in the sub-700 MHz sub-band. As a consequence,
the machine learning algorithm is capable of finding a better fitting for all the
geo-tagged inputs for the mobile cell infrastructure sub-bands (880-915 MHz
and 925-960 MHz). The predicted signal level variation for these segments is
640 up to 8 dB lower for all the simulations (with a mean of approximately 6 dB).

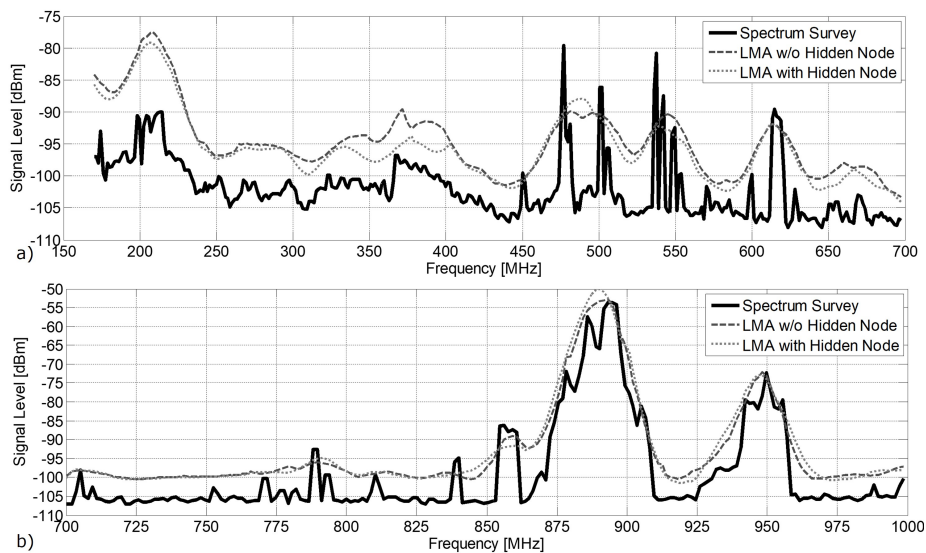


Figure 7: Machine learning performance for minimizing the interference effect caused by hidden nodes in the context of Dynamic Spectrum Access networks. *LMA*: *Levenberg-Marquardt*

4.3. Mitigation of the Interference Effect Caused by Hidden Nodes

Fig. 7 compares the measurements to the machine learning estimation of the mean signal level when a hidden node is emulated. This means, when the signal levels of a certain location are artificially decreased by the shadow margin for mimicking the effect of a hidden node.

Although the effect of the hidden node causes an increase of the machine learning $V_{m_{hn}}$ by 1.1 dB, the interference probability for the TVWS sub-band decreases from 0.0448 to 0. For the case of the above-700 MHz sub-band, the $V_{m_{hn}}$ just increases by 0.4 dB. For the mobile sub-band, if the spectrum allocation is made based on the the Hidden Node data only (i.e., traditional fully distributed DSA networks), the interference probability is 6 times higher compared to our machine learning inference (i.e., 0.0887 versus 0.0148).

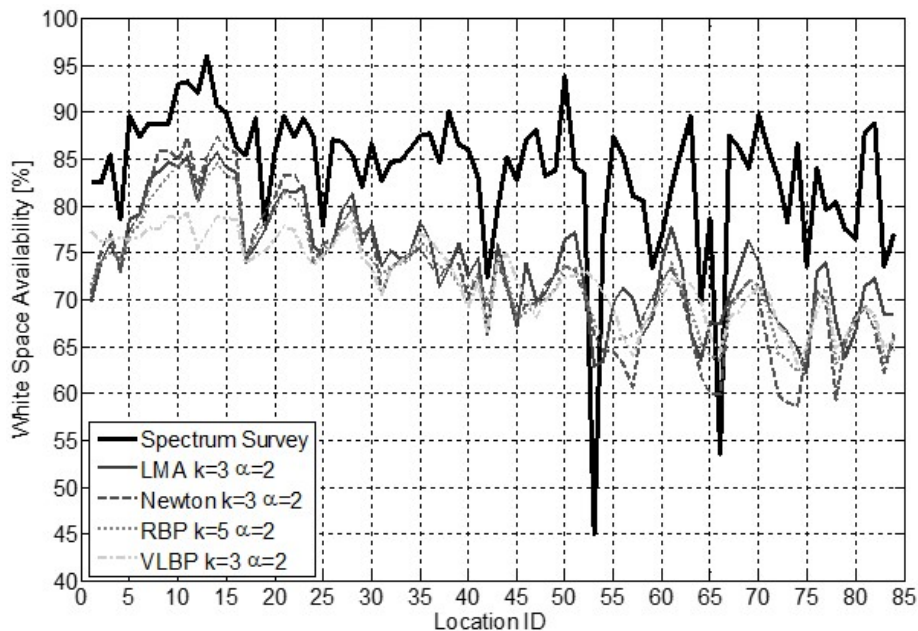


Figure 8: White Space availability calculated from the Spectrum Survey and machine learning estimation for *LMA: Levenberg-Marquardt*, *Newton: Broyden-Fletcher-Goldfarb-Shanno* *Quasi-Newton*, *RBP: Resilient Backpropagation*, *VLBP: Variable Learning Rate Backpropagation*

4.4. Global Quantification of the White Space Availability

Fig. 8 shows the machine learning estimation of the White Space availability
 655 for the evaluated region, considering different training methods compared to the
 results from the measurement campaign (Spectrum Survey). The best machine
 learning performance is obtained for $\alpha = 2$ (ΔW is 2.6% lower compared to
 $\alpha = 1$). For most cases, the best performance and lowest variation is obtained
 for $k = 3$. Most replications of the machine learning for $k = 10$ led to over-
 660 fitting.

Levenberg-Marquardt (LMA) obtained the best results achieving a mean
 White Space availability of 74% (64% for the 95th-percentile). Although the
 Variable Learning Rate Backpropagation (VLBP) led to a similar mean white

space availability (-2% difference), the ΔW metric for some locations is up to
665 7% higher than for the LMA.

The relative Spectrum Utilization efficiency is between 0.62 to 0.67, depend-
ing on the machine learning method. This represents an increase by a factor
6 compared to the current Spectrum Utilization efficiency based on the fixed
allocation of the spectrum (i.e., $SUE = 0.11$ considering the whole surveyed
670 spectrum). The ΔW is always negative (range from -6.27% to -7.12%). This
means that the estimation of spectrum by the machine learning is not at the
cost of over-allocation, and as a consequence the interference probability directly
correlated to the method implementation is relatively low ($P_{Iml} = 0.0238$). In
the surveyed scenario there is a relatively higher gradient in the white space
675 availability for a couple of locations compared to their neighbors. In a scenario
with a more uniform distribution of the white space availability the ΔW might
be lower.

4.5. Hyperparameters Fine Tuning and Computational Performance

The algorithm was evaluated on a PC with a computational power of ap-
680 proximately 15 GFLOPS (i.e., without GPU). Figure 9 shows Algorithm 2 mean
estimation error in dB across 10 simulations for the worst case cluster as a func-
tion of k and α . Because of there were no significant variation in the minimum
number of epochs (except for $\alpha = 10$) we do not analyze this hyperparameter
for the machine learning fine tuning. Here we show the results for the best
685 performing method only (i.e., Levenberg-Marquardt).

The impact in the accuracy is defined by the combinations of both k and α .
As α is inversely proportional to the number of neurons, it has sense that for a
lower number of neurons (higher α) there is a trend to a higher mean error. The
best results (hyperparameter fine tuning) were obtained for $k = 5$ and $\alpha = 1$
690 for the sub-700 MHz segment and $\alpha = 2$ for above 700 MHz (very similar results
for different values of k , i.e., less than 1 dB difference). Notice that in the last
case for $\alpha = 1$ a better fitting of the weights is not reached compared to $\alpha = 2$,
probably due to the limited number of data samples compared to the number

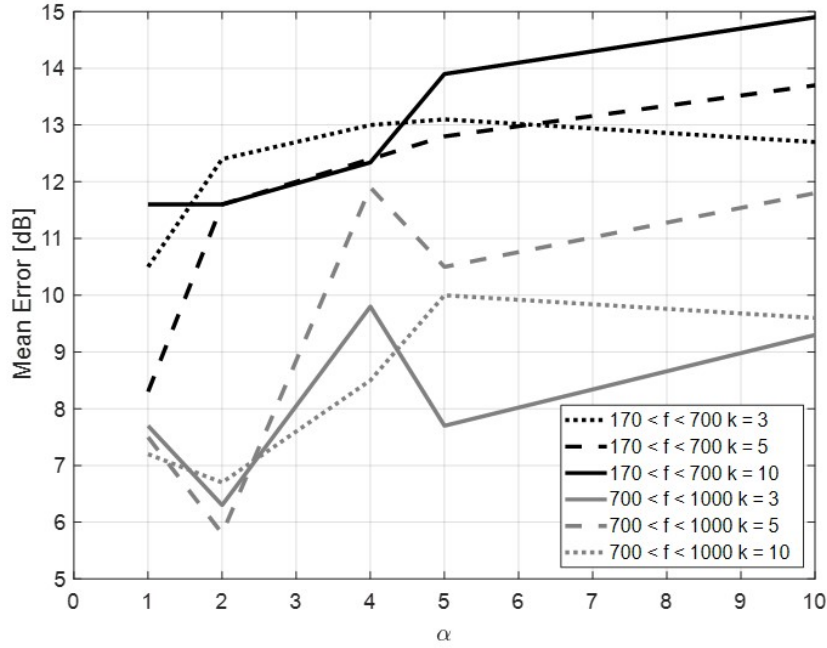


Figure 9: Algorithm mean error for different hyperparameters combinations (k and α). The mean error corresponds to the worst case cluster (with the lowest spectrum correlation) across 10 simulations.

of neurons. Although the best accuracy is achieved for these combinations of hyperparameters, the number of neurons and k-folds have a significant impact on the machine learning performance. Therefore, when choosing the machine learning hyperparameters presented in previous sections we also considered the computational time required for the machine learning training. In any case, because of the gradient descend approximation implemented by this method the error is in most cases a positive value. This means the estimated signal level is above the measured values. Therefore, the interference probability is relatively low and although our machine learning significantly increase the spectrum utilization efficiency, the absolute maximum is not reached.

Figure 10 shows the computational training time for different combinations of the machine learning hyperparameters. For the lower values of α as the number of neurons and weight to fit increases the computational time of the

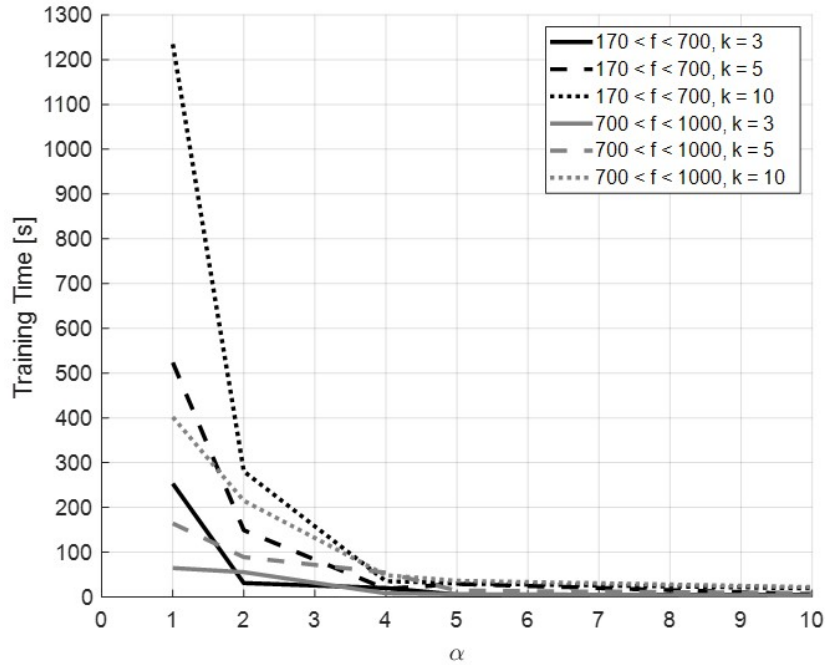


Figure 10: Machine Learning training time for different combinations of hyperparameters (k and α)

algorithm also increase exponentially. The computational time for $k = 10$ compared to $k = 5$ and $k = 3$ is 2 to 9 times higher. For the selected combinations of hyperparameters (i.e., $k = 5$ and $\alpha = 2$ (equivalent to 402 neurons in the hidden layer) for the sub-700MHz and $k=3$ and $\alpha = 2$ (equivalent to 228 neurons in the hidden layer) for above 700 MHz) the average computational time during the training phase was 149 seconds and 55 seconds, respectively. Notice that we account for the spectrum footprint over an extended period of time (i.e., refreshing time much higher than training time by at least an order of magnitude 10). Therefore the machine learning can be trained in the background for dynamically updating the geolocation database. For applications requiring near real-time training, a GPU core might be needed.

Once the data is classified per cluster (i.e., at the *DRU*) and the machine learning is trained, the inference of the spectrum map in any given geo-location

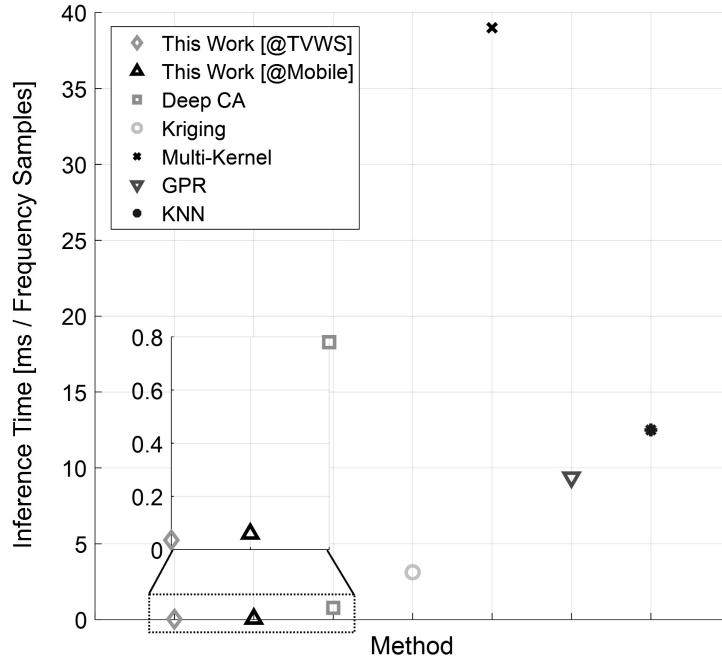


Figure 11: Computational Performance Comparison in terms of inference time in ms divided the number of frequency samples. *Deep CA*: *Deep Completion Autoencoder* [45], *GPR*: *Gaussian Process Regression*, *KNN*: *K-Nearest Neighbor*

720 takes only 12 milliseconds. Fig. 11 shows a comparative analysis in terms of computational efficiency between our algorithms, the deep learning algorithm and other traditional interpolation algorithms benchmarked in [45]. The wireless scenarios evaluated in our paper are more complex than the one evaluated in [45], comprising a larger area, an unknown number of radiating sources, spatial distribution, and bandwidth. For performing an educated guess and fair quantitative comparison we propose as a reference metric the inference time per 725 sampled frequency in the evaluated bandwidth.

Like the deep learning auto-encoder proposed in [45], our trained algorithm does not require additional iterations compared to traditional interpolation 730 methods. The computational time of our feed forward through neural network is 50% less than the computational time of the deep learning auto-encoder

presented in [45], i.e., 12 milliseconds compared to 25 milliseconds. This is despite the fact that the number of frequency samples in our assessment is in the order of 6 to 11 times higher depending on the analyzed spectrum sub-
735 bands. Because of the correlation-based clustering our algorithms have a lower computational time per sampled frequency at least 13 times lower (i.e., higher computational efficiency). This performance is achieved despite the fact that the computational power is approximately 10 times lower than in [45].

5. Conclusion

740 In this paper we investigated the capability of different machine learning methods for estimating the white space availability and maximizing the spectrum utilization efficiency by dynamic spectrum access networks. We designed a heuristic algorithm for validating the reproducibility of our research findings across multiple simulations of the machine learning and validated it with an
745 experimental emulation with data from a real rural environment.

In a distributed DSA network, the proposed machine learning algorithm increase the spectrum utilization efficiency at least 5 times (0.09 to 0.47 for the spectrum licensed to broadcasting television as a primary service). The global estimation of the white space utility shows a higher spectrum utilization
750 efficiency (at least 0.62). However, the spectrum allocation error is on average 9.7% higher compared to the distributed approach.

A cluster classification considering the correlation of the signal level vectors (*spectrum footprints*) at each location with their neighbors allows mitigating the effect of hidden nodes. For the spectrum between 700 MHz and 1 GHz in
755 the surveyed area, the interference probability decreases by a factor 6 compared to the traditional algorithms for the allocation of spectrum in distributed DSA networks.

Future work will consist of a dynamic (real-time) estimation of the spectrum utilization based on unsupervised artificial intelligence implemented through a
760 wireless sensor network. For this, the measured signal levels (tagged output)

will be used for inferring the BS settings (not tagged outputs) that maximize the spectrum utilization efficiency and reduce the interference probability. The mechanism for learning the optimal BS settings will be implemented based on induced measurements of the QoS parameters (i.e, Signal-to-Interference-to-
765 Noise-Ratio).

6. Acknowledgment

Funding: This work was supported by the Flemish Interuniversities Council - University Development Co-operation (VLIR-UOS, Vlaamse Interuniversitaire Raad - Universitaire Ontwikkelingssamenwerking).

770 Grant number: UOSTEA2022001201.

References

- [1] M. Höyhty, A. Mämmelä, M. Eskola, M. Matinmikko, J. Kalliovaara, J. Ojaniemi, J. Suutala, R. Ekman, R. Bacchus, D. Roberson, Spectrum occupancy measurements: A survey and use of interference maps, IEEE
775 Communications Surveys Tutorials 18 (4) (2016) 2386–2414. doi:10.1109/COMST.2016.2559525.
- [2] R. Martinez Alonso, D. Plets, M. Deruyck, L. Martens, G. Guillen Nieto, W. Joseph, Multi-objective optimization of cognitive radio networks, Computer Networks 184. doi:https://doi.org/10.1016/j.comnet.2020.
780 107651.
- [3] S.-M. Kim, J. Kim, H. Cha, M. S. Sim, J. Choi, S.-W. Ko, C.-B. Chae, S.-L. Kim, Opportunism in spectrum sharing for beyond 5g with sub-6 ghz: A concept and its application to duplexing, IEEE Access 8 (2020) 148877–148891. doi:10.1109/ACCESS.2020.3015762.
- 785 [4] IEEE Computer Society, Ieee 802.11af. part 11: Wireless lan medium access control (mac) and physical layer (phy) specifications. amendment 5: Television white spaces (tvws) operation., IEEE, New York, 2013.

- 790 [5] IEEE Computer Society, Ieee 802.22b. part 22: Cognitive wireless ran medium access control (mac) and physical layer (phy) specifications: Policies and procedures for operation in the tv bands., IEEE, New York, 2015.
- [6] G. Barb, F. Alexa, M. Ottesteanu, Dynamic spectrum sharing for future lte-nr networks, *Sensors (Basel)* 21 (12). doi:10.3390/s21124215.
- 795 [7] J. Jeon, R. D. Ford, V. V. Ratnam, J. Cho, J. Zhang, Coordinated dynamic spectrum sharing for 5g and beyond cellular networks, *IEEE Access* 7 (2019) 111592–111604. doi:10.1109/ACCESS.2019.2934385.
- [8] O. Naparstek, K. Cohen, Deep multi-user reinforcement learning for distributed dynamic spectrum access, *IEEE Transactions on Wireless Communications* 18 (1) (2019) 310–323. doi:10.1109/TWC.2018.2879433.
- 800 [9] A. Aragón-Zavala, T. W. C. Brown, G. Castañón, Polarization and effects on hidden node/shadowing margin for tvws, *IEEE Transactions on Broadcasting* 62 (1) (2016) 46–54. doi:10.1109/TBC.2015.2492466.
- [10] J. Martin, L. Dooley, P. Wong, New dynamic spectrum access algorithm for tv white space cognitive radio networks, *IET Communications* 10 (18) (2016) 2591–2597. doi:10.1049/iet-com.2016.0213.
- 805 [11] M. Nitti, M. Murrone, M. Fadda, L. Atzori, Exploiting social internet of things features in cognitive radio, *IEEE Access* 4 (2016) 9204–9212. doi:10.1109/ACCESS.2016.2645979.
- [12] W. Zhang, R. K. Mallik, K. B. Letaief, Optimization of cooperative spectrum sensing with energy detection in cognitive radio networks, *IEEE Transactions on Wireless Communications* 8 (12) (2009) 5761–5766. doi:10.1109/TWC.2009.12.081710.
- 810 [13] J. Tong, M. Jin, Q. Guo, Y. Li, Cooperative spectrum sensing: A blind and soft fusion detector, *IEEE Transactions on Wireless Communications* 17 (4) (2018) 2726–2737. doi:10.1109/TWC.2018.2801833.

- 815 [14] M. Golvaei, M. Fakharzadeh, A fast soft decision algorithm for cooperative spectrum sensing, *IEEE Transactions on Circuits and Systems II: Express Briefs* 68 (1) (2021) 241–245. doi:10.1109/TCSII.2020.3010587.
- [15] R. Sarikhani, F. Keynia, Cooperative spectrum sensing meets machine learning: Deep reinforcement learning approach, *IEEE Communications Letters* 24 (7) (2020) 1459–1462. doi:10.1109/LCOMM.2020.2984430.
- 820 [16] L. Khalid, A. Anpalagan, Adaptive assignment of heterogeneous users for group-based cooperative spectrum sensing, *IEEE Transactions on Wireless Communications* 15 (1) (2016) 232–246. doi:10.1109/TWC.2015.2469667.
- [17] W. Xu, R. Qiu, J. Cheng, Fair optimal resource allocation in cognitive radio networks with co-channel interference mitigation, *IEEE Access* 6 (2018) 37418–37429. doi:10.1109/ACCESS.2018.2845460.
- 825 [18] W. Zhang, C.-X. Wang, X. Ge, Y. Chen, Enhanced 5g cognitive radio networks based on spectrum sharing and spectrum aggregation, *IEEE Transactions on Communications* 66 (12) (2018) 6304–6316. doi:10.1109/TCOMM.2018.2863385.
- 830 [19] S. Yuan, L. Li, C. Chigan, A selfishness-aware coexistence scheme for 802.22 and 802.11af networks, in: *2015 IEEE Wireless Communications and Networking Conference Workshops (WCNCW)*, 2015, pp. 194–199. doi:10.1109/WCNCW.2015.7122553.
- 835 [20] F. Marino, L. Paura, R. Savoia, On spectrum sensing optimal design in spatial-temporal domain for cognitive radio networks, *IEEE Transactions on Vehicular Technology* 65 (10) (2016) 8496–8510. doi:10.1109/TVT.2015.2505087.
- [21] C.-C. Huang, L.-C. Wang, Dynamic sampling rate adjustment for compressive spectrum sensing over cognitive radio network, *IEEE Wireless Communications Letters* 1 (2) (2012) 57–60. doi:10.1109/WCL.2012.010912.110136.
- 840

- [22] J. Zhao, Q. Liu, X. Wang, S. Mao, Scheduled sequential compressed spectrum sensing for wideband cognitive radios, *IEEE Transactions on Mobile Computing* 17 (4) (2018) 913–926. doi:10.1109/TMC.2017.2744621.
- [23] Q. Chen, G. Yu, H. M. Elmaghraby, J. Hamalainen, Z. Ding, Embedding lte-u within wi-fi bands for spectrum efficiency improvement, *IEEE Network* 31 (2) (2017) 72–79. doi:10.1109/MNET.2017.1600034NM.
- [24] C. Politis, S. Maleki, C. G. Tsinos, K. P. Liolis, S. Chatzinotas, B. Ottersten, Simultaneous sensing and transmission for cognitive radios with imperfect signal cancellation, *IEEE Transactions on Wireless Communications* 16 (9) (2017) 5599–5615. doi:10.1109/TWC.2017.2712647.
- [25] X. Liu, C. Sun, W. Yu, M. Zhou, Reinforcement-learning-based dynamic spectrum access for software-defined cognitive industrial internet of things, *IEEE Transactions on Industrial Informatics* 18 (6) (2022) 4244–4253. doi:10.1109/TII.2021.3113949.
- [26] X. Liu, C. Sun, M. Zhou, C. Wu, B. Peng, P. Li, Reinforcement learning-based multislot double-threshold spectrum sensing with bayesian fusion for industrial big spectrum data, *IEEE Transactions on Industrial Informatics* 17 (5) (2021) 3391–3400. doi:10.1109/TII.2020.2987421.
- [27] X. Liu, Q. Sun, W. Lu, C. Wu, H. Ding, Big-data-based intelligent spectrum sensing for heterogeneous spectrum communications in 5g, *IEEE Wireless Communications* 27 (5) (2020) 67–73. doi:10.1109/MWC.001.1900493.
- [28] S. Bhandari, N. Ranjan, Y.-C. Kim, H. Kim, Deep reinforcement learning for dynamic spectrum access in the multi-channel wireless local area networks, in: *2022 International Conference on Electronics, Information, and Communication (ICEIC)*, 2022, pp. 1–4. doi:10.1109/ICEIC54506.2022.9748733.
- [29] Y. Hervis Santana, R. Martinez Alonso, G. Guillen Nieto, L. Martens, W. Joseph, D. Plets, Indoor genetic algorithm-based 5g network planning

using a machine learning model for path loss estimation, *Applied Sciences* 12 (8). doi:10.3390/app12083923.

URL <https://www.mdpi.com/2076-3417/12/8/3923>

- 875 [30] A. A. Asyraf Jainuddin, Y. C. Hou, M. Z. Baharuddin, S. Yussof, Performance analysis of deep neural networks for object classification with edge tpu, in: 2020 8th International Conference on Information Technology and Multimedia (ICIMU), 2020, pp. 323–328. doi:10.1109/ICIMU49871.2020.9243367.
- 880 [31] J. Lee, C. Kim, S. Kang, D. Shin, S. Kim, H.-J. Yoo, Unpu: An energy-efficient deep neural network accelerator with fully variable weight bit precision, *IEEE Journal of Solid-State Circuits* 54 (1) (2019) 173–185. doi:10.1109/JSSC.2018.2865489.
- 885 [32] C.-H. Lin, C.-C. Cheng, Y.-M. Tsai, S.-J. Hung, Y.-T. Kuo, P. H. Wang, P.-K. Tsung, J.-Y. Hsu, W.-C. Lai, C.-H. Liu, S.-Y. Wang, C.-H. Kuo, C.-Y. Chang, M.-H. Lee, T.-Y. Lin, C.-C. Chen, 7.1 a 3.4-to-13.3tops/w 3.6tops dual-core deep-learning accelerator for versatile ai applications in 7nm 5g smartphone soc, in: 2020 IEEE International Solid- State Circuits Conference - (ISSCC), 2020, pp. 134–136. doi:10.1109/ISSCC19947.2020.9063111.
- 890 [33] Y. Z. Ma, *Geostatistical Estimation Methods: Kriging*, Springer International Publishing, Cham, 2019, pp. 373–401. doi:10.1007/978-3-030-17860-4_16.
URL https://doi.org/10.1007/978-3-030-17860-4_16
- 895 [34] R. M. Alonso, A. C. Guerra, E. F. Pupo, D. Plets, G. G. Nieto, L. Martens, W. Joseph, Assessment of white spaces quality in rural areas: a large-scale spectrum survey, in: 2020 IEEE International Symposium on Broadband Multimedia Systems and Broadcasting (BMSB), 2020, pp. 1–5. doi:10.1109/BMSB49480.2020.9379402.

- [35] M. Chen, U. Challita, W. Saad, C. Yin, M. Debbah, Artificial neural
900 networks-based machine learning for wireless networks: A tutorial, *IEEE
Communications Surveys Tutorials* 21 (4) (2019) 3039–3071.
- [36] H. Gavin, The levenberg-marquardt method for nonlinear least squares
curve-fitting problems, Duke University.
- [37] G. Yuan, M. Zhang, Y. Zhou, Adaptive scaling damped bfgs method with-
905 out gradient lipschitz continuity, *Applied Mathematics Letters* 124 (2022)
107634. doi:10.1016/j.aml.2021.107634.
- [38] W. Saputra, T. Tulus, M. Zarlis, R. W. Sembiring, D. Hartama, Analysis
resilient algorithm on artificial neural network backpropagation, *Journal of
Physics: Conference Series* 930 (2017) 012035.
- 910 [39] F. Li, L. Ge, W. Dan, Y. Gu, Q. He, K. Sun, Application of improved vari-
able learning rate back propagation neural network in energy dispersion
x-ray fluorescence quantitative analysis, 2019 IEEE 4th International Con-
ference on Cloud Computing and Big Data Analysis (ICCCBDA) (2019)
428–432.
- 915 [40] Q. Abbas, F. Ahmad, M. Imran, Analysis resilient algorithm on artificial
neural network backpropagation, *Science International (Lahore)* 28 (2016)
2369–2380.
- [41] T.-T. Wong, P.-Y. Yeh, Reliable accuracy estimates from k-fold cross val-
idation, *IEEE Transactions on Knowledge and Data Engineering* 32 (8)
920 (2020) 1586–1594. doi:10.1109/TKDE.2019.2912815.
- [42] ITU-R, Recommendation ITU-R SM.1046-2: Definition of spectrum use
and efficiency of a radio system, ITU, Geneva, Switzerland, 2011.
- [43] R. Martinez Alonso, D. Plets, M. Deruyck, L. Martens, G. Guillen Nieto,
W. Joseph, Dynamic interference optimization in cognitive radio networks
925 for rural and suburban areas, *Wireless Communications and Mobile Com-
puting*doi:10.1155/2020/2850528.

- [44] ETSI., Report TR 103 067: Reconfigurable Radio Systems (RRS); Feasibility study on Radio Frequency (RF) performance for Cognitive Radio Systems operating in UHF TV band White Spaces, ETSI, France, 2013.
- ⁹³⁰ [45] Y. Teganya, D. Romero, Deep completion autoencoders for radio map estimation, *IEEE Transactions on Wireless Communications* 21 (3) (2022) 1710–1724. doi:10.1109/TWC.2021.3106154.